Particle Accelerators
1976, Vol. 7, pp. 125–135

STANFORD'S SUPERCONDUCTING HEAVY ION LINAC STUDY: The Design of Re-Entrant Cavities†

ILAN BEN-ZVI,‡ PETER H. CEPERLEY and H. A. SCHWETTMAN§

High Energy Physics Laboratory and Department of Physics, Stanford University, Stanford, California 94305, USA

(Received June 25, 1973; in final form August 22, 1974)

The design of re-entrant cavities for a superconducting heavy ion accelerator is considered using both approximate and numerical analysis. The approximate analysis of the re-entrant cavities provides a surprisingly good estimate of the electrical and mechanical properties and the transit time factor, and thus it is used to determine the general features of the cavity design. The re-entrant cavity is then optimized using numerical calculations. The properties of an optimized 433 MHz re-entrant cavity, including the quality factor, the R_{sh}/QL-value, the peak electric field, the peak field ratio, the geometric factor, the transit time factor, and the frequency shift values, are calculated numerically and presented.

1 INTRODUCTION

The low particle velocities encountered in a heavy ion accelerator impose important constraints on the design of accelerating structures. The most obvious of these are the necessity of operating at low frequency where beam dynamics problems are less severe, and the necessity of fixing the amplitude and phase of the accelerating fields in each gap of the structure in order to produce the desired velocity profile along the machine. The necessity of operating at low frequency is particularly troublesome for a superconducting heavy ion accelerator since the expensive structure material and the complicated processing techniques severely limit the acceptable physical size of the accelerating structure. One structure which is reasonably compact and therefore suitable for a superconducting heavy ion accelerator is the re-entrant cavity.

A superconducting re-entrant cavity structure exhibits a number of features in addition to its size which could be quite attractive in a heavy ion accelerator.[1] It might, for instance, be possible to design a heavy ion linac as a sequence of independent accelerating gaps, each capable of independent phase and amplitude control. This arrangement would enable one to program the velocity profile along the machine, thus providing complete variability of the beam energy and great flexibility in accelerating ions of different charge-to-mass ratio. For superconducting re-entrant cavities the rf power dissipation is less than one watt, and thus even with heavy beam loading the rf drives can be simple, compact solid-state devices which are efficient, reliable, and inexpensive. A linac which employs independently-controlled accelerating gaps, also provides an excellent opportunity to achieve both phase focusing and radial focusing of the particle beam by alternating the sign of the synchronous phase angle at appropriate intervals along the accelerator length.[2] This method of focusing would eliminate the need for magnetic quadrupoles. In addition, the re-entrant cavity structure, compared to other low-velocity structures, is mechanically rigid, and thus it is less susceptible to the electromechanical instabilities which are important in superconducting heavy ion accelerators.

In this paper we consider the design of superconducting re-entrant cavities, approaching the problem first on the basis of an approximate analysis and then on the basis of numerical calculations. The approximate analysis of the re-entrant

† Work supported by the National Science Foundation under Grant GP33411.

‡ Presently on leave from the Weizmann Institute of Science, Rehovoth, Israel.

§ Alfred P. Sloan Research Fellow.

Editor's Note
The long delay in publication of this paper and of the one that follows has been at the request of the authors who hoped that a third companion paper could have appeared together with these two papers. It is our hope that the third paper on the Stanford superconducting heavy ion linac study can appear in an early issue.

cavity, given in Section 2, provides a surprisingly good estimate of the electrical and mechanical properties and the transit time factor, and it is used to determine the general features of the cavity design. The re-entrant cavity is then optimized using numerical calculations. The properties of an optimized 433 MHz re-entrant cavity that is suitable for accelerating particles with $0.08 < \beta < 0.16$, including the quality factor, the R_{sh}/QL-value, the peak electric field, the peak field ratio, the geometric factor, the transit time factor, and the frequency shift values, are calculated numerically and presented in Section 3 of this paper.

2 APPROXIMATE ANALYSIS OF A RE-ENTRANT CAVITY

Electrical Properties

Although it is not possible to obtain an analytic solution of Maxwell's equations for a re-entrant cavity, Slater[3] has given an approximate analysis which is reasonably accurate if the gap is small compared to the other cavity dimensions. In this approximate analysis the re-entrant cavity is treated as a capacitively loaded section of coaxial line; along the coaxial line the fields are of the form:

$$E_r = \frac{E_0}{r} \sin \frac{2\pi z}{\lambda_0}, \tag{1}$$

$$H_\theta = -j\left(\frac{\varepsilon}{\mu}\right)^{1/2} \frac{E_0}{r} \cos \frac{2\pi z}{\lambda_0}, \tag{2}$$

while in the gap the electric field is:

$$E_z = \frac{2E_0}{g} \ln\left(\frac{r_2}{r_1}\right) \sin \frac{\pi L}{\lambda_0}. \tag{3}$$

As indicated in Figure 1, the quantities g and L are the gap and the length of the cavity, respectively,

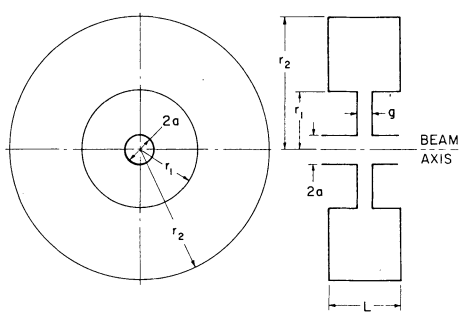

FIGURE 1 Schematic diagram of a re-entrant cavity.

and r_1 and r_2 are the inner and outer cavity radii. The quantity λ_0 is the free space wavelength.

It is shown by Slater that in the limit that $L \ll \lambda_0$ the resonant frequency of the re-entrant cavity, or alternatively the free space wavelength, is given by

$$\lambda_0 = r_1\left[\frac{2\pi^2}{g/L} \cdot \ln\left(\frac{r_2}{r_1}\right)\right]^{1/2}. \tag{4}$$

The tuning sensitivity of the re-entrant cavity can be found by differentiating Eq. (4). For a change in the cavity gap

$$\frac{\Delta f}{f} = \frac{1}{2}\frac{\Delta g}{g}, \tag{5a}$$

and for a change in the cavity length

$$\frac{\Delta f}{f} = -\frac{1}{2}\frac{\Delta L}{L}, \tag{5b}$$

The rf power that must be coupled into a re-entrant cavity in order to develop a voltage $V = E_z g$ across the gap is given by

$$P = \frac{V^2}{(R_{sh}/Q)Q_0}. \tag{6}$$

The R_{sh}/Q-value, where R_{sh} is the cavity shunt resistance, is

$$\frac{R_{sh}}{Q} = \left(\frac{\mu}{\varepsilon}\right)^{1/2} \cdot \frac{L/\lambda_0}{\ln(r_2/r_1)}, \tag{7}$$

and the unloaded cavity Q is

$$\frac{1}{Q_0} = \frac{R}{\Gamma} = \frac{2R}{\omega\mu}\left\{\frac{1/r_1 + 1/r_2}{2\ln(r_2/r_1)} + \frac{1}{L}\right\}, \tag{8}$$

where R is the surface resistance and Γ is the geometric factor.

In cavity experiments we determine Q_0 and the coupled power P, and from these we calculate the stored energy $U = PQ_0/\omega$. The stored energy is related to the fields through

$$U = \frac{\varepsilon\pi r_1^2}{2g} V^2 = \frac{\varepsilon\pi r_1^2 g}{2} E_z^2 \tag{9a}$$

and

$$U = \frac{\mu\lambda_0^2 g}{2\pi} H^2(r_1). \tag{9b}$$

Breakdown Optimization

In an accelerator it is important to achieve as large a voltage gradient as practical. Since magnetic breakdown and electron field emission can limit

the voltage gradient in superconducting cavities, it is essential that the re-entrant cavity be designed to minimize the electric and magnetic fields on the walls.

If in practice one is limited by magnetic breakdown, then the quantity

$$\Gamma_H \equiv \frac{V/L}{H_{\max}} \tag{10}$$

should be maximized in the cavity design. Since the magnetic field is weak in the region of the gap, the maximum magnetic field can be calculated from Eq. (2):

$$H_{\max} = \left(\frac{\varepsilon}{\mu}\right)^{1/2} \frac{E_0}{r_1}. \tag{11}$$

The voltage across the gap of the re-entrant cavity is $V = E_z g$, and thus combining Eqs. (3), (10), and (11) we get

$$\Gamma_H = 2\pi\left(\frac{\mu}{\varepsilon}\right)^{1/2} \frac{r_1}{\lambda_0} \ln\left(\frac{r_2}{r_1}\right). \tag{12}$$

For given λ_0 and r_2, Γ_H has a maximum for $r_2/r_1 = e$. If in practice one is limited by electron field emission, then the quantity

$$\Gamma_E \equiv \frac{V/L}{E_{\max}}, \tag{13}$$

should be maximized in the cavity design. As we shall see in Section 3, in a well-designed re-entrant cavity $E_{\max} = V/g$, and thus Γ_E is just g/L. From Eq. (4) then

$$\Gamma_E = \frac{2\pi^2}{\lambda_0^2} r_1^2 \ln\left(\frac{r_2}{r_1}\right), \tag{14}$$

and for given λ_0 and r_2, Γ_E has a maximum for $r_2/r_1 = e^{1/2}$.

Consider a re-entrant cavity with a 35-cm diameter and a 2-cm gap that is resonant at 433 MHz. The two optimization conditions lead to the dimensions and fields given in Table I, assuming in each case a voltage gradient V/L of 3 MV/m.

Experiments on superconducting cavities, particularly at low frequencies,[4] indicate that field emission is the more serious limitation on field strength. Therefore we adopt the ratio $r_2/r_1 = e^{1/2}$ as our optimum. This choice of r_2/r_1 also gives the smallest cavity diameter for a given frequency as can be seen from Eq. (4).

TABLE I

Parameters of optimized re-entrant cavities

	$r_2/r_1 = e$	$r_2/r_1 = e^{1/2}$
λ_0 (cm)	69.15	69.15
V/L (MV/m)	3.0	3.0
r_2 (cm)	17.5	17.5
r_1 (cm)	6.4	10.6
g (cm)	2.0	2.0
L (cm)	11.8	8.6
$E_{\max}$ (V/cm)	1.8×10^5	1.3×10^5
$H_{\max}$ (G)	172	208

Approximate Transit Time Factor

It is important to find the energy gain of a particle going across the gap at a velocity $v = \beta c$. Following the treatment of Chambers[5] we express the field parallel to the axis as a Fourier integral:

$$E_z(r, z, t) = E(r, z)\cos \omega t = \int_0^\infty B(r, k, t)\cos kz \, dk. \tag{15}$$

The Fourier coefficient $B(r, k, t)$ satisfies the Bessel equation and with axial symmetry is of the form:

$$B(r, k, t) = A(k) I_0(ar)\cos \omega t, \tag{16}$$

where $a^2 = k^2 - (\omega/c)^2$. Here $A(k)$ is independent of r and t, and I_0 is the modified Bessel function. It is convenient to express the Fourier coefficient as

$$B(r, k, t) = \frac{2}{\pi} I_0(ar) \int_0^\infty E(0, z)\cos \omega t \cos kz \, dz$$

$$= \frac{1}{\pi} \frac{W}{e} \cos \omega t I_0(ar) T(k). \tag{17}$$

The quantity $W = e \int_{-\infty}^{\infty} E(0, z)\, dz$ is the maximum energy gain of an infinite velocity particle, and $T(k)$ is defined by

$$T(k) = \frac{e}{W} \int_{-\infty}^{\infty} E(0, z)\cos kz \, dz. \tag{18}$$

Now the energy gained by a particle of charge e is just

$$\Delta K = e \int_{-\infty}^{\infty} E_z(z, \omega t_p)\, dz, \tag{19}$$

where $\omega t_p = \omega z/v - \phi$, and using Eqs. (15) and (17) this can be written:

$$\Delta K = \frac{W}{\pi} \int_0^\infty dk T(k) I_0(ar) \int_{-\infty}^{\infty} dz \cos \omega t \cos kz \tag{20}$$

We can now integrate Eq. (20) with the result:

$$\Delta K = WT(k_1)I_0(a_1 r)\cos\phi, \tag{21}$$

where

$$k_1 = \frac{\omega}{v} = \frac{2\pi}{\beta\lambda}, \quad \text{and} \quad a_1^2 = k_1^2 - \left(\frac{\omega}{c}\right)^2 = \left(\frac{2\pi}{\beta\lambda}\right)^2 - \left(\frac{2\pi}{\lambda}\right)^2.$$

For $\beta^2 \ll 1$ we have $a_1 = k_1$. The quantity $T(k_1)$ is the transit time factor.

In order to evaluate the transit time factor for simple geometries, we have to find an analytic expression for E_z. Let us take a gap and beam tube geometry as shown in Figure 1, where g is the gap length and a is the beam tube radius. Since in a re-entrant cavity g and a are much less than λ_0, an electrostatic approximation for the field is satisfactory. In addition, we will make a two-dimensional approximation, solving for E_z in the (r, z) plane by the use of conformal mapping techniques. Following Weber,[6] we start with a known electric field solution to E in the complex u plane given by

$$E_z = E_p\left\{\frac{1-u^2}{p^2-u^2}\right\}^{1/2} \tag{22}$$

where $E_p = V/g$, and $p = [1 + (2a/g)^2]^{1/2}$. As explained by Weber, the u plane can be related to the (r, z) plane through a rather complicated conformal mapping. However along the beam axis where $r = 0$, this transformation is much simpler and is defined by:

$$\frac{dz}{du} = -\frac{g}{\pi}\frac{(p^2-u^2)^{1/2}}{1-u^2} = -\frac{g}{\alpha\pi}\frac{(1-\alpha^2u^2)^{1/2}}{1-u^2}, \tag{23}$$

where $\alpha = 1/p$. By substituting $u = \sin x$, Eq. (23) can be integrated, yielding

$$z = \frac{g}{\alpha\pi}\left\{\frac{\beta}{2}\ln\left[\frac{(1-\alpha^2u^2)^{1/2}+\beta u}{(1-\alpha^2u^2)^{1/2}-\beta u}\right] + \alpha \arcsin \alpha u\right\} \tag{24}$$

with $\beta = (1-\alpha^2)^{1/2}$. We can now write Eq. (22) in the form

$$E_z = \frac{E_p}{p}\cdot\frac{1}{\cosh\left(\frac{\pi z}{2a} + \frac{g}{2a}\arcsin\frac{u}{p}\right)}. \tag{25}$$

For large z we have

$$E_z \approx \frac{E_p}{p}\cdot\frac{1}{\cosh\frac{\pi z}{2a}}, \tag{26}$$

and for small z we have

$$E_z \simeq \frac{E_p}{p}\frac{1}{\cosh\left(\frac{2\pi a z}{g^2p^2}\right)}. \tag{27}$$

From the large z and the small z approximations to the axial electric field given in Eqs. (26) and (27), we can generate a suitable interpolation formula. Our interpolation formula for the axial electric field is

$$E_z = \frac{E_p}{\left[1+\left(\frac{2a}{g}\right)^2\right]^{1/2}\cosh\left[\frac{\pi z}{(g^2+4a^2)^{1/2}}\right]}. \tag{28}$$

Equation (28) gives a good description of E_z for $2a \geq g$. While it is not quite as good for $2a < g$, it is still comparable to the usual square-field approximation which is good for $2a \ll g$.

Now we can calculate the transit time factor using Eqs. (28) and (18). The integration can be done analytically, and the only error will come from the approximations leading to Eq. (28):

$$T(k_1) = \frac{1}{\cosh\left[\frac{\pi(g^2+4a^2)^{1/2}}{\beta\lambda_0}\right]}. \tag{29}$$

This approximate expression for the transit time factor can be compared to the expression for the square-field approximation:

$$T(k_1) = \sin\frac{(\pi g)}{\beta\lambda_0}\Big/\frac{\pi g}{\beta\lambda_0}. \tag{30}$$

Frequency Tuning

The frequency of a re-entrant cavity can shift as a result of changes in atmospheric pressure, changes in radiation pressure, and changes in the position of a mechanical tuner. In this section we derive approximate expressions for these frequency changes and then in Section 3 test them against a more accurate computer calculation in a specific case.

To facilitate the proposed calculations, we will make certain simplifying approximations. First we will assume that only the gap g and the length L are affected by the detuning mechanisms. The justification for this assumption is the mechanical stability of the re-entrant cavity against changes in r_1 and r_2. Second, we will assume that the cavity members are bent linearly. Thus the deformation is given by two parameters: δ_L is the amount by which

the cavity length changes at $r = r_1$ while at r_2 there is no change, and δ_g is the relative gap change between $r = a$ and $r = r_1$.

Now we proceed to calculate the frequency change in terms of δ_L and δ_g. The time-averaged radiation pressure at any point on the surface of the cavity is given in terms of the magnitude of surface field:

$$P_R = \tfrac{1}{4}(\varepsilon E^2 - \mu H^2). \tag{31}$$

From Slater's perturbation method[3] we have

$$\frac{\Delta f}{f} = \frac{1}{4U}\int(\mu H^2 - \varepsilon E^2)\,dv, \tag{32}$$

where the integration extends over the perturbed volume. Using Eq. (31) in Eq. (32), we get

$$\frac{\Delta f}{f} = -\frac{\Delta W}{U}, \tag{33}$$

where ΔW is the work done by the radiation force when the cavity boundary is displaced. To calculate ΔW we have to express the radiation pressure in terms of the cavity parameters. Using the approximate expressions derived for the re-entrant cavity we find:

$$P_{R,\text{gap}} = \frac{U}{2\pi r_1^2 g}\left[1 - \left(\frac{\pi r}{\lambda_0}\right)^2\right], \tag{34a}$$

$$P_{R,\text{coax}} = -\frac{U}{4\pi r^2 L \ln\dfrac{r_2}{r_1}}. \tag{34b}$$

Integrating this pressure over the perturbed volume defined by the deflections δ_g, δ_L we obtain an expression for ΔW which, upon insertion into Eq. (33) yields

$$\frac{\Delta f}{f} = \delta_L\left[\frac{1}{g}\left(1 - \frac{g}{4L\ln\dfrac{r_2}{r_1}}\right) - \frac{1}{L}\left(\frac{r_2}{r_2 - r_1} - \frac{1}{\ln\dfrac{r_2}{r_1}}\right)\right] + \delta_g\left(1 - \frac{3g}{20L\ln\dfrac{r_2}{r_1}}\right)\Bigg/\left[3\left(1 - \frac{a}{r_1}\right)g\right]. \tag{35}$$

This approximate expression for the relative frequency shift is applicable independent of whether the deflection is the result of radiation pressure, the result of atmospheric pressure, or the result of an external force exerted by a mechanical tuner.

We must now express δ_L and δ_g in terms of the perturbing forces. For uniform pressures, P_{gap} and P_{coax}, applied to the cavity walls we get[7]

$$\delta_g = -P_{\text{gap}}S\left[r_1^4 + 3a^4 - 4r_1^2a^2\left(1 + \ln\frac{r_1}{a}\right) + \frac{16r_1^2a^4}{r_1^2 - a^2}\left(\ln\frac{r_1}{a}\right)^2\right], \tag{36a}$$

$$\delta_L = -P_{\text{coax}}S\left[r_2^4 + 3r_1^4 - 4r_2^2r_1^2\left(1 + \ln\frac{r_2}{r_1}\right) + \frac{16r_2^2r_1^4}{r_2^2 - r_1^2}\left(\ln\frac{r_2}{r_1}\right)^2\right] - \frac{4}{\pi}P_{\text{gap}}[r_1^2 - a^2] \times\left[r_2^2 - r_1^2 - \frac{4r_1^2r_2^2}{r_2^2 - r_1^2}\left(\ln\frac{r_2}{r_1}\right)^2\right], \tag{36b}$$

while for a force F applied along the beam tube we get

$$\delta_g = -\frac{4}{\pi}SF\left[r_1^2 - a^2 - \frac{4r_1^2a^2}{r_1^2 - a^2}2\left(\ln\frac{r_1}{a}\right)^2\right], \tag{37a}$$

and

$$\delta_L = -\frac{4}{\pi}SF\left[r_2^2 - r_1^2 - \frac{4r_1^2r_2^2}{r_2^2 - r_1^2}\left(\ln\frac{r_2}{r_1}\right)^2\right]. \tag{37b}$$

In these equations S is a strength parameter of the cavity walls, given by

$$S = \frac{3(m^2 - 1)}{16m^2Yt^3} \tag{38}$$

The quantity m is the reciprocal Poisson's ratio, which we take as 2.63 for niobium at low temperatures, Y is Young's modulus taken as 1.27×10^{11} newtons/m^2, and t is the wall thickness, taken as 0.5 cm, and thus $S = 0.96 \times 10^{-5}$ (N-m)$^{-1}$. Equations (36a) and (36b) are appropriate to use for atmospheric pressure and for radiation pressure, while Eqs. (37a) and (37b) are appropriate to use for a mechanical tuner.

For the optimized cavity studied in Section 3 we can now calculate the frequency shifts associated with changes in atmospheric pressure, changes in radiation pressure, and changes in the force

exerted by a mechanical tuner. For the case of atmospheric pressure $P_{gap} = P_{coax} = P$, and from Eqs. (35) and (36) we get

$$\frac{1}{P}\frac{\Delta f}{f} = -8.08 \times 10^{-6}\,(\text{Torr})^{-1}. \tag{39}$$

For the case of radiation pressure, P_{gap} and P_{coax} can be calculated as the appropriate average of Eqs. (34a) and (34b), and combining these with Eqs. (35) and (36) gives us

$$\frac{1}{U}\frac{\Delta f}{f} = -2.51 \times 10^{-5}\,(\text{J})^{-1}. \tag{40}$$

Similarly, for a mechanical tuner pushing with a force F we use Eqs. (35) and (37) and get

$$\frac{1}{F}\frac{\Delta f}{f} = -2.49 \times 10^{-6}\,(\text{N})^{-1}. \tag{41}$$

In Section 3 we will compare these results with numerical calculations worked out for the same model cavity.

Electromechanical Instability

The extremely narrow bandwidth of superconducting cavities leads to the possibility of electromechanical instabilities.[8–10] These instabilities can occur when the frequency shift due to radiation pressure exceeds the bandwidth, so that the resonance curve becomes overhanging, as shown in Figure 2. In this case, the lower frequency side of resonance is statically unstable; when the cavity is operated at frequency f_1, as shown in Figure 2, the cavity can be filled to point (c) but not to point (b). The higher frequency side of resonance, indicated as point (a), is statically stable, but is subject to

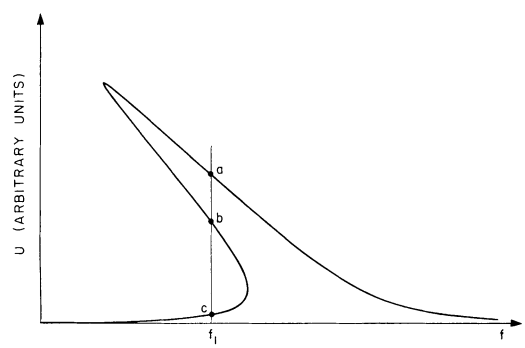

FIGURE 2 Overhanging resonance curve which occurs when the frequency shift due to radiation pressure exceeds the bandwidth.

ponderomotive oscillations, a dynamic instability in which radiation pressure drives a mechanical resonance in the cavity walls. Ponderomotive oscillations result in periodic variations of the cavity resonant frequency accompanied by a modulation of the rf field level and thus must be prevented to allow stable operation of an accelerator.

The mechanism responsible for ponderomotive oscillations can be understood by considering the effect that vibrations of the cavity walls has on the cavity fields. Associated with wall vibration there is an oscillation of the cavity resonant frequency. If the cavity is being operated on the sloping portion of its resonance curve, the frequency oscillation results in modulation of the rf energy level in the cavity and consequently in modulation of the radiation pressure exerted on the cavity walls. Depending on the relative phase, this oscillating part of the radiation pressure either drives or dampens the initial mechanical vibration. If the cavity is operated on the high-frequency side of the resonance curve, such vibrations are always driven, and if the radiation pressure is strong enough, the oscillations are self sustaining.

Because both types of electromechanical instabilities are a result of radiation pressure which in turn is proportional to the amount of rf energy stored in the cavity, there is a minimum rf energy required for their occurrence. This stored energy level is called the threshold energy U_{Th}, and is given by

$$U^d_{Th} = (2K_jQ_jQ_E)^{-1}\,\frac{[(1-\xi^2+\eta^2)^2+4\xi^2]}{4\xi\eta}, \tag{42}$$

for ponderomotive oscillations where $\xi > 0$, and by

$$U^s_{Th} = \frac{(2K_0Q_E)^{-1}(1+\xi^2)}{(-2\xi)}, \tag{43}$$

for static instability where $\xi < 0$. The quantities f_j, K_j and Q_j are the resonant frequency, the electromechanical coupling constant, and the mechanical Q of the jth mechanical resonance of the cavity. The quantities f_0 and Q_E are the rf resonant frequency and rf loaded Q of the cavity. The normalized tuning error ξ which appears in Eqs. (42) and (43) is defined by the relation

$$\xi = \frac{2Q_E(f-f_0)}{f_0}, \tag{44}$$

where f is the rf generator frequency. The normalized mechanical frequency η is similarly defined as

$$\eta = \frac{2Q_E f_j}{f_0}. \tag{45}$$

The static electromechanical coupling constant, K_0, is the normalized static shift of the cavity resonant frequency due to radiation pressure:

$$K_0 = \frac{1}{U}\frac{\Delta f_0}{f_0}, \tag{46}$$

and is calculated in Eq. (40) to be $-2.51 \times 10^{-5}(\mathrm{J})^{-1}$ for our re-entrant cavity. K_0 is related to the dynamic K's by

$$K_0 = \sum_j K_j. \tag{47}$$

In the case of the re-entrant cavity one would expect the sum of the K_j's to be dominated by the first mechanical mode, and thus for most calculations one can approximate Eq. (47) as $K_1 \approx K_0$. The first mechanical resonant frequency of a re-entrant cavity is given by[11]

$$f_1 = 0.9342\,\frac{t}{2r_2^2}\left[\frac{Ym^2}{\rho(m^2-1)}\right]^{1/2}, \tag{48}$$

where $\rho = 8.6 \times 10^3\ \mathrm{kg/m^3}$ is the density of niobium. For our example cavity, $f_1 = 330$ Hz.

Because of the extremely narrow bandwidth of superconducting cavities, mechanical vibrations of the cavity walls can easily lead to large tuning errors. In such a case one is interested in the minimum threshold energy for varying tuning error. For high Q superconducting cavities where $\eta = 2Q_E f_1/f_0 \gg 1$, the minimum threshold energy for ponderomotive oscillations is

$$\mathrm{Min}[U_{Th}^d] = (2K_j Q_j Q_E)^{-1}, \tag{49a}$$

and occurs at $f = f_0 + f_j$. The minimum threshold energy for static instabilities is

$$\mathrm{Min}[U_{Th}^s] = (2K_0 Q_E)^{-1}, \tag{49b}$$

and occurs at $f = f_0 - f_0/2Q_E$. This minimum value of U_{Th}^s corresponds to the lowest rf energy at which the resonance curve becomes overhanging. Equations (49a) and (49b) indicate that $\mathrm{Min}[U_{Th}^d] = Q_M^{-1}\,\mathrm{Min}[U_{Th}^s]$, so that if Q_M is greater than one, as it usually is, a cavity is more unstable against ponderomotive oscillations than against static instabilities. Thus ponderomotive oscillations can occur even before the curve becomes overhanging. Assuming $Q_M = 100$ and $Q_E = 10^8$, and the previously stated values of K_0, f_1 and f_0, we get

$$\mathrm{Min}[U_{Th}^s] = 0.2\ \mathrm{mJ}, \tag{50a}$$

and

$$\mathrm{Min}[U_{Th}^d] = 2.0\ \mu\mathrm{J}. \tag{50b}$$

The minimum threshold energy for ponderomotive oscillations is quite small compared to the energy (0.5 J) stored in a re-entrant cavity for an accelerator gradient of 3 MV/m. However, this minimum occurs at $f = f_0 + f_1$ which is 75 cavity bandwidths off resonance. A more realistic value of U_{Th}^d is obtained by considering a $\mathrm{Min}[U_{Th}^d]$ for a smaller range of tuning errors. For a smaller range of tuning errors where $\eta \gg 1$ and $\eta \gg \xi$,

$$\mathrm{Min}[U_{Th}^d] = \frac{(2K_j Q_j Q_E)^{-1}\eta^3}{4\xi}. \tag{51}$$

In the case of our re-entrant cavity, this yields $\mathrm{Min}[U_{Th}^d] = 0.6$ J, at $|\xi| \leq 3$ or 1.5 bandwidths off resonance. Thus we see that in this range of tuning error, the cavity is completely stable against ponderomotive oscillations up to an accelerator gradient of 3 MV/m.

Equation (50a) indicates that the cavity is statically unstable. One can stabilize it by using an electronic feedback circuit to level the rf fields in the cavity. To be effective the open loop gain of the feed-back system must be at least as large as the ratio of the cavity energy to the threshold energy, U/U_{Th}^s, which in this case equals 2.5×10^3. In addition, the feedback system must respond to disturbances of frequencies up through

$$f_d = \left(\frac{f_0}{2Q_E}\right)(1+\xi^2)^{1/2}, \tag{52}$$

with less than a 90° lag in response. In our case f_d equals 7 Hz for $|\xi| = 3$. Thus the cavity can be stabilized using an electronic leveling system with an open loop gain of 2.5×10^3 and a gain bandwidth product of $(2.5 \times 10^3) \times (7\ \mathrm{Hz}) = 18$ kHz. These seemingly mild requirements are complicated by the fact that the cavity introduces a pole in the feedback system at 4.3 Hz and the fact that the cavity may be operated 1.5 bandwidths off resonance, at which point the gain of the leveling system is reduced from its on-resonance value. These effects increase the gain and bandwidth requirements of the leveling circuitry to 2.5×10^4

and 180 kHz respectively. However, these requirements should be quite easy to meet, if one uses a direct rf feedback system.

3 NUMERICAL ANALYSIS OF A RE-ENTRANT CAVITY

Shape Optimization

Once the general shape of the cavity has been determined, we can solve Maxwell's equations numerically, and perturb the cavity boundaries to improve the cavity properties. The numerical analysis is done with the Los Alamos computer program LALA.[12] A sectional view of a re-entrant cavity which is designed for particles with $0.08 \leq \beta \leq 0.16$ is shown in Figure 3. The design frequency is 433 MHz. It is obvious that the surface electric field is large in the re-entrant part of the cavity, and that a sharp edge anywhere in this region will enhance the local field, without contributing to the total voltage gain across the gap. The ideal situation is a surface field which is constant along the re-entrant portion of the cavity at a value E_p, for then the total voltage gain across the gap will be $V = E_p g$. The object of the numerical study is to design a cavity at 433 MHz, with a gap $g = 2$ cm, a beam tube diameter $2a = 2$cm, and a cavity diameter $2r_2 = 38$ cm, which has a nearly uniform peak surface electric field.

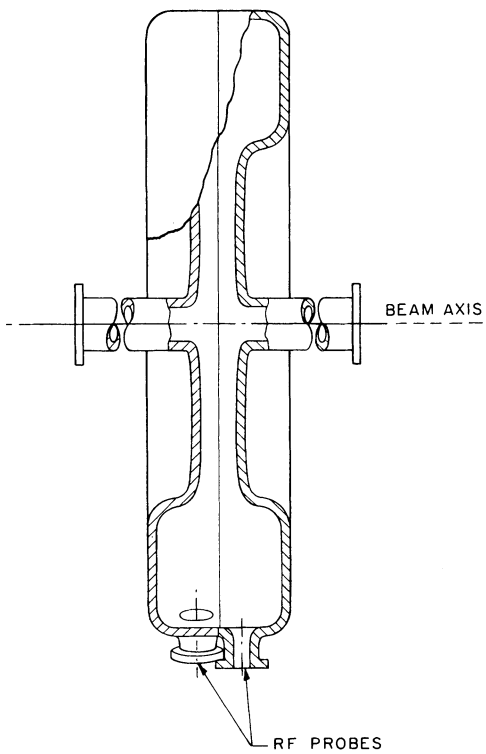

FIGURE 3 Sectional view of the 433 MHz re-entrant cavity.

Since the LALA program is limited to treating boundaries made of sections of ellipses (including circles) and straight lines, the principle behind the search for an optimum boundary is quite simple. Where the field is peaked, the radius of curvature of the boundary section in question is increased, or the radial distance of the section from the center is increased. It turns out that a rather simple sequence of boundary sections in the re-entrant part of the cavity yields satisfactory results; the boundary consists of a tapered straight line, joined at both ends to quarter ellipses. A proper choice of the taper, the length of the line, and the ellipse axes and centers limits the surface field variation to less than 4 percent.

The boundary of the optimized re-entrant cavity using the LALA format is described in Table II. In the LALA format a line section is described by the coordinates (ZB1, RB1) of a point at the start of the line and the coordinates (ZB2, RB2) of a point at the end of a line. An ellipse section is described by the coordinates (ZC, RC) of the ellipse center and by the length of the axes, R1 and R2, along the Z and R directions respectively. Positive values of R1 and R2 imply counter-clockwise ellipse sections and negative values imply clockwise sections. All coordinates are given in centimeters. The surface electric field distribution for the optimized cavity is given in Figure 4. As we can see from the flatness of the field distribution along the re-entrant part, this

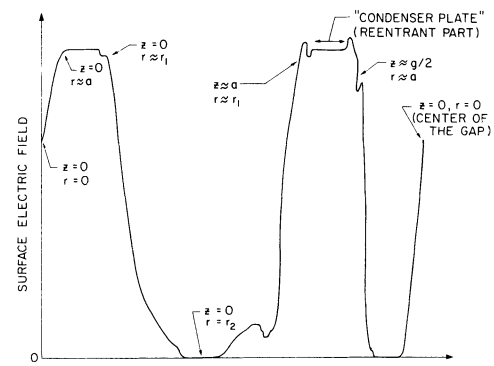

FIGURE 4 Surface electric field distribution for the optimized 433 MHz re-entrant cavity.

boundary is quite good. In fact, the figure of merit

$$\left(\frac{1}{E_p g}\right)\int_{-\infty}^{\infty} E_z \, dz,$$

as calculated from the computer results is unity, and thus we can use the peak surface electric field for acceleration with 100 percent efficiency.

The fast drop of the surface field, evident in Figure 4, on going from the re-entrant part of the cavity to the beam tube is achieved by making the semi-minor axis of the ellipse which describes that boundary section as small as possible. The limit on this process is obviously local surface field enhancement. In Table II we find this axis under R1(8) and it is 0.5 cm. The practical significance of this fast drop can be understood when we consider the manufacturing process of the cavity. Nearly one half of the cavity can be made from a single sheet of niobium metal in a single forming operation. The beam tube has to be welded to this formed section. In re-entrant cavity experiments it is found that good internal electron beam welds which are machined after welding to produce a smooth surface, yield surface imperfections after chemical polishing. The position of the beam tube weld can be moved out of the high-field region by a drawing operation which pulls the center of the formed section along the ellipse contour. However, the amount by which this can be done is limited, and thus it is necessary to design a fast drop of the field in this region. The numerical calculations show that at the point where the straight section of the beam tube starts [point ZB1(9), RB1(9) in Table II] the surface field has dropped already to 15 percent of E_p.

The only other weld in this cavity is on its equator where the two halves are joined to form one cavity. Although the electric field is zero at this point, the magnetic field is finite. The numerical calculations of the surface magnetic field, given in Figure 5, however, show that the ratio (field at the weld)/(maximum field) is only 0.69. This situation is also quite favorable.

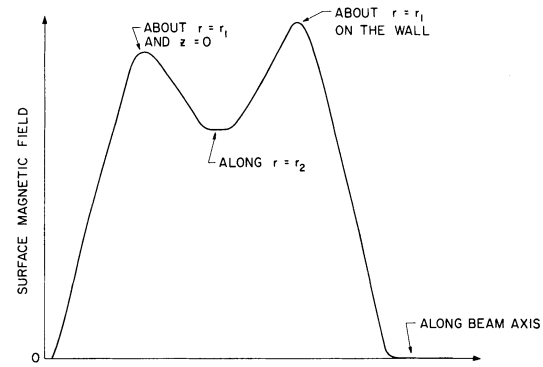

FIGURE 5 Surface magnetic field distribution for the optimized 433 MHz re-entrant cavity.

Electrical Properties and Transit Time Factor

The electrical parameters of the optimized re-entrant cavity given in Table II have been calculated using the LALA program. Calculated values of the cavity frequency, the quality factor, the R_{sh}/QL-value, the peak electric field, the peak field ratio, the geometric factor, and the transit time factor are given in Table III and compared there to values predicted for this cavity by the approximate analysis of Section 2. The agreement between the approximate values calculated analytically and the rather accurate numerical calculations is quite good. Thus one can design a re-entrant cavity using the various approximate

TABLE II

Cavity boundary parameters (LALA format) for optimized cavity

No.	RB1	ZB1	RB2	ZB2	RC	ZC	R1	R2
1	0	0	17.5	0	—	—	—	—
2	17.5	0	17.5	2.5	—	—	—	—
3	17.5	2.5	16.5	3.5	16.5	2.5	−1.0	−1.0
4	16.5	3.5	12.8	3.5	—	—	—	—
5	12.8	3.5	10.5	2.2	11.8	2.2	−1.3	−1.3
6	10.5	2.2	7.5	1.0	7.8	2.2	1.2	2.6
7	7.5	1.0	3.0	1.05	—	—	—	—
8	3.0	1.05	1.0	1.55	3.0	1.55	0.5	2.0
9	1.0	1.55	1.0	4.0	—	—	—	—
10	1.0	4.0	0	4.0	—	—	—	—
11	0	4.0	0	0	—	—	—	—

TABLE III

Electrical parameters of optimized 433 MHz cavity

Quantity	Symbol	Units	Numerical	Approximate	Equation
Frequency	F	MHz	437.18	442	(5)
Quality factor[a]	Q	—	1.247×10^4	1.10×10^4	(6)
R_{sh}/QL	—	Ω/m	706.9	1087	(13)
Peak electric field	$E_p/(PQ)^{1/2}$	$\frac{\text{V}}{\text{m} \times \text{W}^{1/2}}$	356.6	344	(12*b*)
Peak field ratio	E_p/H_p	$\frac{\text{V}}{\text{m} \times \text{0e}}$	6.67×10^4	6.9×10^4	(11*a*)
Geometric factor	Γ	Ω	67	60	—
Transit time factor[b]	T	—	0.64	0.51	(33)

[a] The quality factor is calculated using the conductivity for copper at room temperature ($\sigma = 0.591 \times 10^8$ MHO/meter).

[b] The transit time factor is calculated for particles with $\beta = 0.1$.

expressions given in Section 2, evaluating the various electrical properties with reasonable confidence before doing any computer work.

The axial field distribution for the re-entrant cavity is given in Figure 6. Curve (a) represents the numerical calculation using the LALA program, while curve (b) represents the exact electrostatic solution given by Eqs. (22) and (24) and curve (c) represents the approximate electrostatic solution [Eq. (28)] which is used to calculate the transit time factor of Eq. (29). The difference between curves (a) and (b) are due mainly to the rounding of the gap edges. The numerical transit time factor in Table III is calculated directly from the axial field distribution given by curve (a). It is interesting to note that the approximate result of Eq. (29) underestimates this value by 20 percent, while the square-field approximation of Eq. (30), if an effective gap $(g^2 + 4a^2)^{1/2}$ is assumed, overestimates the transit time factor by 20 percent.

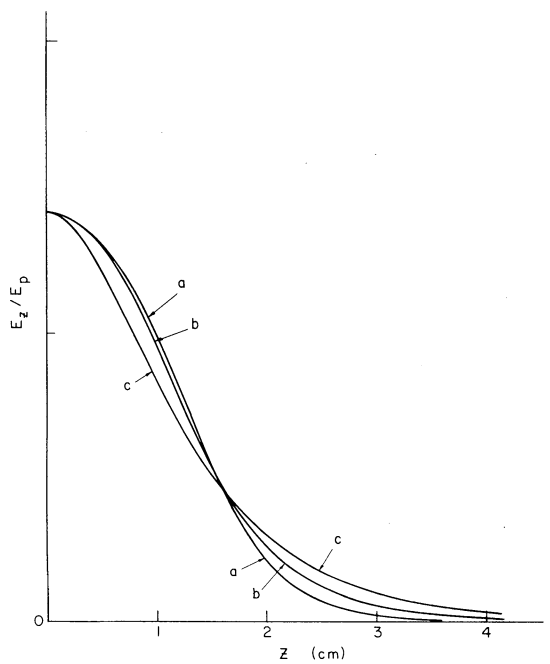

FIGURE 6 Numerical and approximate axial electric field distribution for the optimized 433 MHz re-entrant cavity.

In comparing superconducting structures an appropriate figure of merit is $R_{sh}\Gamma/LQ$ since for given surface resistance this quantity relates the power dissipated per unit length to the voltage gradient. For a helix R_{sh}/LQ is on the order of 3000 Ω/m which is much larger than the 707 Ω/m calculated for the re-entrant cavity. However, the geometric factor is on the order of 7 Ω for the helix compared to 67 Ω for the re-entrant cavity, and thus the figure of merit for the helix is approximately one half that for the re-entrant cavity.

Frequency Tuning

For our optimized re-entrant cavity (see Table II) we can compare the approximate results of Section 2 for the frequency tuning with numerical calculations. The deformation of the cavity walls can be calculated using the computer program "NONLIN".[13] The required input to the program, in addition to the boundary description, is the detailed load distribution. For atmospheric pressures the load distribution is uniform, for radiation pressure

TABLE IV

Approximate and numerical frequency shift values

Effect	Magnitude	Work ΔW (lb/inch)	$\Delta W/U$	Shift	Numerical	Approximate	Equation
Atmospheric pressure	1 Torr	36.76×10^{-6}	10.40×10^{-6}	$\frac{1}{p}\frac{\Delta f}{f}$ Torr^{-1}	-10.4×10^{-6}	-8.1×10^{-6}	(46)
Radiation pressure	0.399 J	35.60×10^{-6}	10.08×10^{-6}	$\frac{1}{U}\frac{\Delta f}{f}$ J^{-1}	-25.3×10^{-6}	-25.1×10^{-6}	(47)
Mechanical tuner	1 lb	111.30×10^{-6}	31.52×10^{-6}	$\frac{1}{F}\frac{\Delta f}{f}$ N^{-1}	-6.95×10^{-6}	-2.5×10^{-6}	(48)

the load distribution must be calculated using the electromagnetic fields obtained from the LALA program, and for the mechanical tuner the load distribution is confined to the beam tube. The work done on the electromagnetic fields in the cavity is calculated from the local deformation of the cavity wall and the local radiation pressure and from this the frequency shift is obtained. Table IV summarizes the results. The agreement between the approximate expressions developed in Section 2 and the numerical calculation is remarkably good, with the exception of mechanical tuner result, which is more than a factor of 2 off.

Mechanical tuning of the re-entrant cavity can be accomplished in a number of ways. One possibility is to use a stack of piezoelectric crystals. For a commercially available crystal such as Clevite Corp. PZT-4, a stack of 100 crystals and a voltage range of ± 400 V provides a frequency tuning range of $\Delta f/f \simeq \pm 1.5 \times 10^{-5}$ which is equivalent to a pressure change of about ± 1.5 Torr, or a cavity energy change of about ± 0.6 J.

ACKNOWLEDGEMENT

The authors wish to thank R. R. Cochran of the Stanford Linear Accelerator Center for his great help which made the frequency tuning calculations possible.

REFERENCES

1. I. Ben-Zvi, P. H. Ceperley and H. A. Schwettman, High Energy Physics Laboratory Report No. 731, Stanford University, Stanford, Calif. (1974). To be published in *Particle Accelerators*.
2. E. E. Chambers and I. Ben-Zvi, *Particle Accelerators*, this issue, p. 137.
3. J. C. Slater, *Microwave Electronics* (D. Van Nostrand Co., New York, 1950), p. 232.
4. I. Ben-Zvi, J. G. Castle, Jr. and P. H. Ceperley, *IEEE Trans. Nucl. Sci.* **NS-19**, No. 2, 226 (1972).
5. E. E. Chambers, High Energy Physics Laboratory Report No. 653, Stanford University, Stanford, Calif. (1971).
6. E. Weber, *Electro-Magnetic Fields, Vol. 1* (John Wiley and Sons, New York, 1950), pp. 352–353.
7. R. J. Roark, *Formulas for Stress and Strain* (McGraw-Hill, New York, 1965), p. 222.
8. D. Schulze, *Proc. 1970 Proton Linear Accelerator Conference*, **1**, 259 (1970), National Accelerator Laboratory, Batavia, Illinois.
9. P. H. Ceperley, *IEEE Trans. Nucl. Sci.* **NS-19**, No. 2,217 (1972).
10. P. H. Ceperley, High Energy Physics Laboratory Report No. 655, Stanford University, Stanford, Calif. (1971).
11. P. M. Morse, *Vibration and Sound* (McGraw-Hill, New York, 1948), p. 210.
12. H. C. Hoyt, *Rev. Sci. Instr.* **37**, 755 (1966).
13. T. M. Trainer *et al.* Final report on the Development of Analytical Techniques for Bellows and Diaphragm Design, Battelle Memorial Institute, Columbus Labs. Report No. AFRPL-TR-68-22. Air Force Rocket Propulsion Lab. Res. and Tech. Div., A. F. Systems Command, Edwards A. F. B., California.